Transport of spring floodwater from rivers under ice to the Alaskan Beaufort Sea

Matthew B. Alkire[1,2] and John H. Trefry[1]

Received 16 December 2005; revised 24 March 2006; accepted 3 July 2006; published 9 December 2006.

[1] Spring floods carry Alaskan river water north to a frozen Beaufort Sea. A plume of water from the Sagavanirktok River (SR) was identified and traced by measuring salinity, $\delta^{18}O$, and dissolved silica in discrete water samples collected beneath landfast ice in the coastal Alaskan Beaufort Sea from late May to early June 2004 during high river flow. An Optimum Multiparameter analysis was used to calculate the fractions of SR water from the measured geochemical parameters. The SR plume followed the northwestward flowing local circulation and moved ~17 km north and ~15 km west under ice from the river mouth. The river plume was ~1–1.5 m thick beneath the ice and flowed above a persistent halocline in the top 2.5 m of the water column. The calculated volume of SR water beneath the ice on 2 June was ~0.5 km^3, approximately 50% of the river discharge during the study period. The volume of water that was not accounted for was assumed to flow above the ice canopy or was not captured during the study. Interactions of SR water with another under-ice plume from the Kuparuk River resulted in increased northward transport of both freshwater discharges.

Citation: Alkire, M. B., and J. H. Trefry (2006), Transport of spring floodwater from rivers under ice to the Alaskan Beaufort Sea, *J. Geophys. Res.*, *111*, C12008, doi:10.1029/2005JC003446.

1. Introduction

[2] Small North American rivers with annual discharges less than the Mackenzie River (~300 km^3) or the Yukon River (~200 km^3) [*Aagaard et al.*, 1981], such as the Colville River (~15 km^3) [*Rember and Trefry*, 2004], are often ignored or excluded in freshwater budgets. However, these rivers can transport freshwater, dissolved chemicals, and land-borne contaminants relatively long distances (~20 km) offshore during the spring melt because the seasonal cover of landfast ice inhibits mixing by winds and waves [*Ingram*, 1981; *Walker*, 1998; *Weingartner and Okkonen*, 2001; *Granskog et al.*, 2005]. Independently, small rivers do not contribute significantly to the freshwater budget of the Arctic. Yet, the numerous rivers present along the Alaskan and Canadian coastlines may be collectively entrained into larger and stronger flows known to move off the shelf, such as the Mackenzie River plume or the Alaskan Coastal Current. Conversely, river water that is not advected off the shelf can retain its distinct geochemical signature and move with the local circulation [*Granskog et al.*, 2005]. If these residual waters remain on the shelf, they can mix with additional freshwater from the melting of sea ice and further freshen the shelf water and subsequent brines produced from ice formation the following winter [*Macdonald et al.*, 1995, 1999; *Eicken et al.*, 2005].

[3] This study was designed to identify and trace the plume of the Sagavanirktok River (SR) beneath the ice during spring floods to identify general flow patterns for freshwater, dissolved chemicals, and potential contaminants originating from the North Slope of Alaska. The North Slope is an active area for oil exploration and production, both onshore and offshore, that has yielded >14 billion barrels of oil since 1977 that were transported from Prudhoe Bay to Port Valdez via the 1300-km-long Trans-Alaskan Pipeline [*Sever*, 2005]. Therefore under-ice freshwater plumes are important components of spill trajectories as well as biogeochemical models during the period of maximum river discharge.

[4] In addition to lower salinity, Alaskan Arctic rivers have higher concentrations of dissolved silica and lighter oxygen isotope ratios than ambient shelf water and sea-ice meltwater [*Macdonald et al.*, 1989, 1995]. These geochemical tracers provide a distinct fingerprint that can be used to characterize SR water exclusively and therefore describe both the progression of the plume under ice as well as its interactions with additional water masses in the study area. The tracer data were combined into an Optimum Multiparameter (OMP) analysis to calculate fractions of these water masses in discrete samples of seawater.

2. Background

2.1. Study Area

[5] This study was conducted in Stefansson Sound, a small and shallow area (average water depth <15 m) located

[1]Department of Marine and Environmental Systems, Florida Institute of Technology, Melbourne, Florida, USA.
[2]Now at College of Oceanic and Atmospheric Sciences, Oregon State University, Corvallis, Oregon, USA.

0148-0227/06/2005JC003446

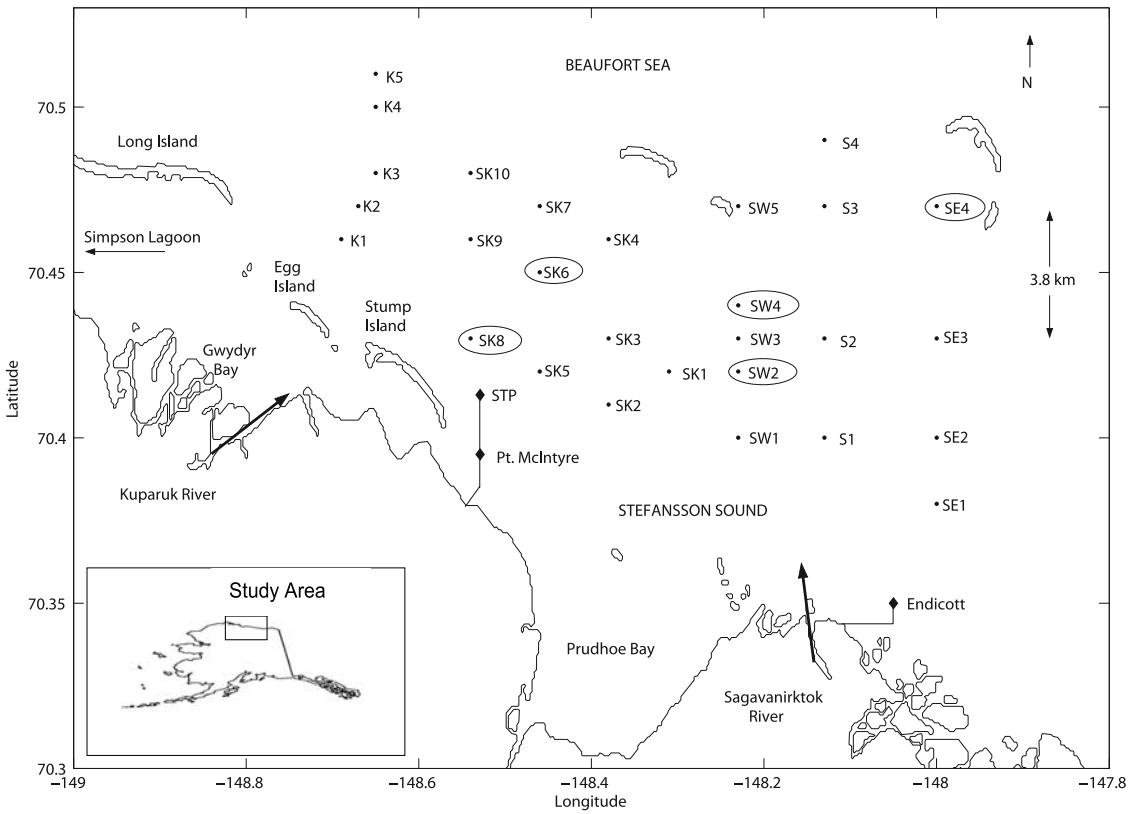

Figure 1. Sampling sites in Stefansson Sound with inset map of Alaska showing study area. Causeways connecting the Seawater Treatment Plant (STP), Pt. McIntyre, and Endicott Island to shore are shown by the solid lines. Stations numbers in ovals identify locations where ice cores also were collected. Arrows show approximate direction of primary river outflow. Map of coastline from the *National Geophysical Data Center* [2005].

offshore of the North Slope of Alaska and partially protected by barrier islands that separate it from the Beaufort Sea (Figure 1). Seasonal landfast ice (~2 m thick) that covers the area from October through April begins to melt in late May and eventually breaks up and blows offshore in July [*Weingartner and Okkonen*, 2001]. During the spring melt, Alaskan Arctic rivers, including the SR, flow at maximum discharge above and below the landfast ice. The ambient shelf water has a salinity that can range from 20 (July–September) to 35 annually, with average values of 31–32 in spring as observed during the present study. Water temperatures of −1.6° to −1.8°C during winter increase to as high as 4°C during the summer open water period [*Weingartner and Okkonen*, 2001]. Salinities ≥34 have been observed in winter by *Weingartner and Okkonen* [2001] in Stefansson Sound and were attributed to the presence of brine. The absence of water with salinity >32 during this study suggests either mixing of brines with ambient shelf water or lateral transport off the shelf. The shelf water is referred to here as the Polar Mixed Layer (PML), a term adopted from *Macdonald et al.* [1989]. Circulation in the study area varies with the season as the presence of the ice determines the influence of winds on water movement. The area has a tidal range of ~0.2 m with currents that range from <1 to 24 cm s^{-1} and average 2 cm s^{-1}, with <10% of the current magnitudes >10 cm s^{-1} during the landfast ice period [*Matthews*, 1981; *Weingartner and Okkonen*, 2001].

[6] Details on the seasonal discharge and the specific geologic makeup of the SR drainage basin have been discussed or referenced by *Rember and Trefry* [2004]. Briefly, the frozen tundra and snowpack upstream begin to melt during spring and slowly flow downstream (northward), melting the SR in route. The meltwater carries particulate and dissolved components frozen in the ice and snow from the previous year as it flows downstream, weathering exposed rock and additional soil layers from the surrounding river banks. This thawing and weathering contributes to the specific chemical composition of the river. During high discharge, that lasts only 1–2 weeks, Alaskan Arctic rivers typically transport 40–80% and >80% of their total annual discharge of water and suspended sediment, respectively [*Rember and Trefry*, 2004]. Figure 2 shows the mean daily streamflow of the SR during the year of 2004 with predominant flow during the spring floods and scattered summer rain storms.

2.2. Scale and Comparison of Under-Ice Plumes

[7] Relatively few studies have investigated the flow of Arctic river plumes under ice to the ocean [*Macdonald et al.*, 1995, 1999; *Eicken et al.*, 2005; *Granskog et al.*, 2005] or large bays [*Ingram*, 1981; *Ingram and Larouche*, 1987; *Ingram et al.*, 1996]. Within these studies, key differences in the scale and seasonality of discharge are observed. The total annual input of SR water to Stefansson Sound in 2004

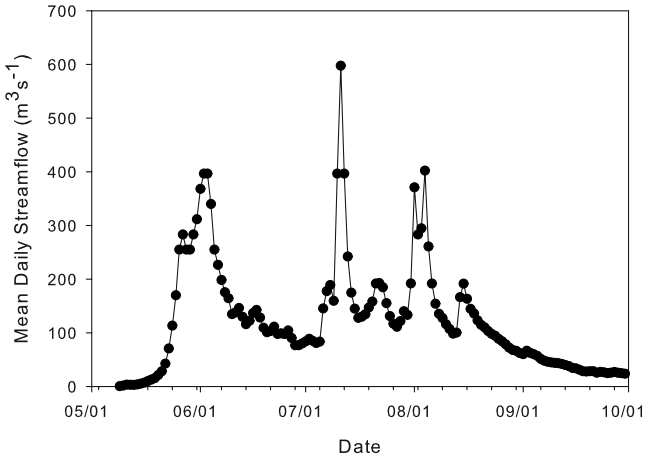

Figure 2. Mean daily streamflow for the SR in 2004. Values prior to early June were extrapolated because of a lack of measurements during the initial spring floods. Data from *USGS* [2005].

was estimated from *U.S. Geological Survey (USGS)* [2005] data as ~8 km^3. This value is very small, for example, compared to total annual input of 330 km^3 for the Mackenzie River [*Macdonald et al.*, 1999] and 520 km^3 for the Lena River [*Aagaard and Carmack*, 1989], but larger than that for the Siikajoki River, 1.2–1.4 km^3 [*Granskog et al.*, 2005]. Man-made causeways, on-site laboratories, bridges, and various modes of transportation facilitate sample collection and processing with an enhanced degree of safety in a very challenging environment to study, particularly during the spring freshet. Therefore the SR provides a valuable analogue for the study of the flow of relatively smaller Arctic rivers under ice.

[8] Following the spring floods of the SR, the landfast ice layer breaks up and initializes the summer open water period, during which mixing of the ambient shelf water with runoff and sea-ice meltwater (SIM) remaining on the shelf reduces stratification in Stefansson Sound, producing a relatively homogenous layer from which sea ice will form in mid-October. Therefore the fraction of the spring discharge remaining on the shelf will have an impact on the salinity of brines produced the following winter [*Melling and Moore*, 1995]. The lack of any significant river runoff from the SR during winter months provides an opportunity for a more saline surface layer by eliminating the "snowplow" mechanism that captures brine rejected from the ice during formation as observed in the Mackenzie estuary [*Macdonald et al.*, 1995]. Therefore the freshwater component of the shelf in winter will depend upon the distribution of SIM and spring runoff, which varies annually depending on the details of the spring break up, winds, and local circulation following the maximum river discharge in May–June.

3. Methods

3.1. Sampling

[9] River water, seawater, and ice cores were collected from 23 May to 2 June 2004 during the landfast ice period while rivers were at high flow. River water was sampled daily at the same sites studied by *Rember and Trefry* [2004]. Seawater was collected through holes drilled in the ice at 28 stations using a peristaltic pump equipped with acid washed Tygon tubing (Table 1 and Figure 1). Sampling through the ice was limited to nine days by the time of onset of the floods, weather conditions, and accessibility when nearshore areas flooded above the ice. Samples were collected at depths of 0.5, 1, 1.5, 2.5, 4, 6, 7, and 10 meters below the ice layer, depending on the depth of the water column under the ice. Samples were collected ~20–30 min after drilling the hole to allow for reestablishment of any stratification in the water column. The tubing was flushed at a rate of 4 L min^{-1} with sample water for several minutes before collection at each depth to permit at least a two-fold rinse of the complete tube. River water and seawater samples were collected in low-density polyethylene bottles (0.5 L) that were prewashed with 10% HCl and rinsed with distilled, deionized water (DDW). Bottles were rinsed 3 times with sample before collection. Ice cores were collected at stations SW2, SW4, SE4, SK6, and SK8 (Figure 1) to determine end-member values for SIM. Ice cores were obtained using a Sipre corer and auger with a hollow center, then they were sectioned in situ into five 30–40 cm intervals and melted in separate containers in the dark over ~24 hours.

[10] All samples were returned to an on-site laboratory near Prudhoe Bay, filtered and subsampled within 24 hours. Unfiltered samples of water were poured off to determine salinity and the remaining water was vacuum filtered through acid-washed polycarbonate filters (0.4 μm pore size). The first 50 mL of the filtrate were discarded as an additional rinse of the filtration system. Then, samples for $\delta^{18}O$ and dissolved silica were collected. Silica samples were stored at 4°C until analysis.

3.2. Analysis

[11] Salinity was calculated from the measured chlorinity of the discrete water samples using the Mohr titration as described by *Grasshoff* [1976]. Calculated salinities were checked by analyzing a subset of samples (n = 34) using a Guideline 8400-B salinometer at the National Oceanic and Atmospheric Administration (NOAA) laboratory in Miami. The correlation coefficient for the salinities determined by both methods was 0.999. Concentrations of dissolved silica were determined within 48 hours of collection via the molybdenum blue spectrometric method [*Grasshoff*, 1976]. Reagent blanks and laboratory replicates were analyzed for quality control and precision (Table 2). Values for $\delta^{18}O$ were determined for 62 samples from key stations that were selected on the basis of salinity and dissolved silica values. Analyses were conducted by Geochron Laboratories, Inc. using a VG Micromass gas source stable isotope ratio mass spectrometer and results were reported as referenced to VSMOW (Vienna Standard Mean Ocean Water). Analytical precision for $\delta^{18}O$ was 0.1‰ and a strong correlation (r^2 = 0.996) was found versus salinity as described below. Current magnitudes and directions were measured and averaged at selected depths at each station using an AANDERAA Doppler current meter. Data are reported only for those sites where at least three consecutive current directions differed by <30°. Precision was estimated

Table 1. Coordinates, Sampling Dates, Water Depths Under Ice, and Ice Thicknesses for Water Stations Occupied During 2004

Station	Latitude, N	Longitude, W	Sample Date	Water Depth, m	Ice Thickness, m
SE1	70°22.97′	147°59.99′	27 May	4.2	1.9
SE2	70°24.00′	147°59.98′	27 May	4.6	1.7
SE3	70°26.00′	148°00.00′	27 May	4.9	2.4
SE4	70°28.00′	148°00.00′	27 May	3.8	1.9
S1	70°24.00′	148°08.00′	27, 31 May	3.2	1.9
S2	70°25.86′	148°08.00′	31 May	4.8	1.8
S3	70°28.00′	148°08.00′	31 May	4.0	1.9
S4	70°29.60′	148°08.03′	31 May	9.1	1.9
SW1	70°24.23′	148°13.98′	25 May	2.3	1.9
SW2	70°25.00′	148°13.98′	25, 28 May	3.2	1.9
SW3	70°25.79′	148°13.96′	25 May	5.0	1.8
SW4	70°26.59′	148°13.97′	25, 28, 31 May	6.3	1.9
SW5	70°28.19′	148°13.93′	28 May	2.3	2.0
SK1	70°25.00′	148°18.80′	25, 28 May	2.0	2.2
SK2	70°24.49′	148°22.97′	30 May	1.2	2.0
SK3	70°25.83′	148°22.98′	28 May	4.6	1.9
SK4	70°27.45′	148°22.99′	30 May	5.5	2.0
SK5	70°25.12′	148°27.64′	30 May	2.9	2.0
SK6	70°26.75′	148°27.65′	29 May, 2 June	3.2	1.9
SK7	70°28.36′	148°27.65′	30 May	5.1	1.9
SK8	70°25.60′	148°32.50′	30 May, 2 June	3.2	1.9
SK9	70°27.72′	148°32.50′	29 May	7.0	1.9
SK10	70°29.04′	148°32.46′	30 May	7.7	1.7
K1	70°27.66′	148°41.29′	23 May	5.1	1.9
K2	70°28.32′	148°40.07′	23 May	7.3	1.9
K3	70°29.00′	148°38.78′	24, 29 May	8.7	1.8
K4	70°29.80′	148°38.74′	29 May	10.0	1.9
K5	70°30.60′	148°38.89′	29 May	11.0	1.9

to be ±1.6 cm s^{-1} and ±9° for speed and direction, respectively.

3.3. OMP Analysis

[12] Optimum multiparameter analysis, a weighted, nonnegative, linear least squares mass balance, was used to calculate the relative fractions of each water mass in a discrete sample based on methods from *Karstensen* [2005]. Briefly, the method finds the best fitting fraction (x) of ($n + 1$) water types that contribute to the (n) observed values of the selected tracers in a water sample via solution of an overdetermined system of linear equations that minimized the residual error. Boundary conditions were applied to the method to guarantee that all fractions calculated were positive and that the sum of all fractions was 100% (mass conservation). Three specific tracers (salinity, $\delta^{18}O$, and dissolved silica) were combined with the assumption of mass conservation as a fourth variable to quantify the fractions of three water masses that contributed most to each individual station.

[13] The success of the OMP method is dependent upon accurate end-member values [*Thompson and Edwards*, 1981; *Tomczak*, 1981a, 1981b; *Mackas et al.*, 1987]. An initial end-member matrix was calculated by averaging all measurements for each parameter sampled directly from the four water masses (Table 3). Final values were chosen by fine tuning the initial end-members within the range of analytical precision and daily variability in accordance with *Mackas et al.* [1987]. This procedure yielded end-members with the lowest residuals in the calculated water mass fractions (Table 3). Additional details regarding the determination of end-member values are given in section 4.1.

[14] The end-member matrix and sample observations were multiplied by a diagonal weight matrix to account for differences in tracer reliability, environmental variability, and precision and accuracy of the data. *Thompson and Edwards* [1981] used estimates of analytical precision to determine tracer weights, whereas *Mackas et al.* [1987] and *Macdonald et al.* [1989] based weights on measurement uncertainty and the variance and covariance of tracer properties in a given area. In this study, the method for allocating weights was adapted from *Mackas et al.* [1987] and *Hinrichsen and Tomczak* [1993] and involved the following: (1) multiplying the estimated analytical precision by a factor of ten, (2) dividing by the range of end-member values, and (3) taking the inverse to yield weights of 30 for salinity, $\delta^{18}O$, and mass conservation (assumed equal to largest weights), and 10 for dissolved silica.

[15] An estimate of the error associated with the calculation was necessary to determine the quality of the water

Table 2. Data for Absolute Precision, Precision as Coefficient of Variation (CV), and Accuracy for Chemical Analyses of Tracers

Measurement	Precision[a]	CV, %	Accuracy,[b] %	Reference Material
Salinity, ‰	±0.1 (n = 35)	1.6 (n = 35)	±0.5 (n = 25)	IAPSO seawater
Dissolved silica, μM	±0.3 (n = 20)	2.0 (n = 20)	±0.5 (n = 18)	J.T. Baker stock solution
$\delta^{18}O$, ‰	±0.1 (n = 9)	2.6 (n = 9)	- -	VSMOW

[a]Absolute precision was calculated as the average standard deviation from analysis of duplicate and triplicate samples.
[b]Accuracy was calculated as the percent relative error with respect to the listed reference materials.

Table 3. Initial and Final (bold) Values of End-Members for Water Masses[a]

Water Mass	Salinity	δ^{18}O, ‰	Dissolved Silica, μM
Kuparuk River (KR)	0.02 ± 0.01 (n = 7) **0.0**	−23.0 ± 0.3 (n = 4) **−23.0**	13 ± 1 (n = 8) **14.0**
Sagavanirktok River (SR)	0.12 ± 0.02 (n = 8) **0.0**	−21.7 ± 0.4 (n = 4) **−21.7**	24 ± 5 (n = 9) **25.0**
Meteoric Water[b]	0.15	−20.3	46.5
Sea-ice melt (SIM)	5.0 ± 0.9 (n = 19) **5.0**	−0.8 ± 0.1 (n = 2) **−0.8**	0.9 ± 0.5 (n = 19) **0.0**
Sea-ice melt[b]	5.0	−2.4	2
Polar Mixed Layer (PML)	31.1 ± 0.6 (n = 71) **32.1**	−3.4 ± 0.1 (n = 6) **−3.4**	8 ± 1 (n = 70) **8.0**
Polar Mixed Layer[b]	31.6	−3.5	4.7

[a]Final values are bold.
[b]From *Macdonald et al.* [1989].

mass fractions yielded from this analysis. On the basis of suggestions by *Karstensen* [2005], *Macdonald et al.* [1989], and *Hinrichsen and Tomczak* [1993] this problem was approached in the following ways: (1) varying end-member definitions and weights, (2) adding random, equally distributed white noise (±1σ) to sample observations, (3) varying the specific water masses included in each calculation, and (4) calculating water mass fractions using only salinity and silica without weighting or normalization. Using these comparisons, water mass fractions in each sample were estimated to be accurate to ±10%, which was similar to that estimated by *Macdonald et al.* [1989]. Error residuals associated with the accepted water mass fraction calculations are listed in Table 4.

4. Results and Discussion

4.1. Tracers

[16] Salinity, δ^{18}O and dissolved silica provided distinct geochemical fingerprints to calculate the relative contributions of four water masses to individual water samples via OMP analysis. Temperature was excluded as a tracer because of the small range between end-members (−1.8° to 0.5°C), daily variations in rivers (±0.1° to 0.5°C), and solar heating of surface waters, as previously observed by *Macdonald et al.* [1989]. In addition, errors associated with the OMP calculations increased significantly when temperature was included in the end-member matrix.

[17] End-member values were determined using samples of river water, seawater, and sea-ice collected during the study period because these values can vary annually and over the melt season [*Rember and Trefry*, 2004]. The locations of river sampling sites downstream provide data that integrate the total river signal, including variations in tributaries and in snowmelt, and thus provide a reasonable estimate of the isotopic signature of the runoff flowing into Stefansson Sound during spring floods. The δ^{18}O values for ice collected at two extreme locations (SE4 and SK8, Figure 1) and depths in the ice core (0–30 cm and 144–188 cm) were −0.7 and −0.9‰. The mean value of −0.8‰ has a fractionation offset from the PML (δ^{18}O = −3.4‰) of +2.6‰, the same offset found by *Macdonald et al.* [1995] for the Canadian Beaufort Sea. The salinity of the ice samples (n = 19) was relatively uniform at 5.0 ± 0.9, suggesting that the ice was generally homogeneous within the study area during 2004.

[18] The strong linear relationship between salinity and δ^{18}O, coupled with marked differences in end-member values for each parameter, yielded two variables that clearly supported discrimination between river water and seawater (Figure 3). However, the data for salinity and δ^{18}O could not be used to effectively differentiate SR from Kuparuk River (KR) water. Despite daily variations in the concentrations of dissolved silica for the SR (Table 3), silica could be used (1) to distinguish between water from the SR and KR (Figure 4) and (2) to better define the contribution from SIM because SIM contained very low concentrations of dissolved silica relative to the other three water masses (Table 3 and Figure 4). Some of the data points that plotted

Table 4. Error Residuals for Accepted Water Mass Fractions Calculated for Selected Transects[a]

Transect of Stations	AMR, %	MMR, %	Salinity	Silica, μM	δ^{18}O, ‰
SW 1,2,3,4 and SK1	0.2	1.1	0.1	0.8	0.1
SW 2,4,5 and SK1	0.3	1.6	0.1	1.3	0.2
K 1,2,3	0.2	0.7	0.0	0.4	0.1
K 3,4,5	0.3	1.1	0.0	0.8	nd
SE 1,2,3,4 and S1	0.6	1.4	0.1	1.5	nd
S 1,2,3,4	1.1	4.3	0.2	4.8	nd
SK 2,3,4	0.2	0.7	0.3	1.1	0.1
SK 5,6,7	0.3	0.8	0.4	1.2	0.1
SK 8,9,10	0.2	0.7	0.3	1.0	0.3

[a]Average mass residuals (AMR) and maximum mass residuals (MMR) were calculated from the absolute values of the data set. Missing δ^{18}O residuals are for those stations without data.

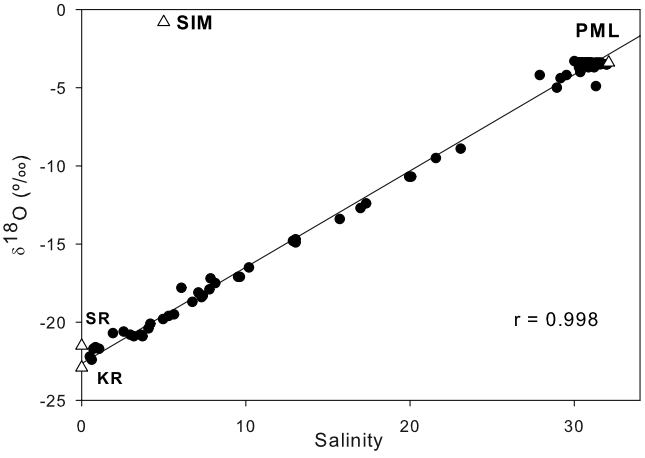

Figure 3. Salinity versus δ^{18}O for selected stations in Stefansson Sound from 23 to 31 May 2004. End-member values for SR, KR, SIM, and PML are shown by the open triangles and labeled accordingly. The linear regression line is shown, and the correlation coefficient (r) was 0.998.

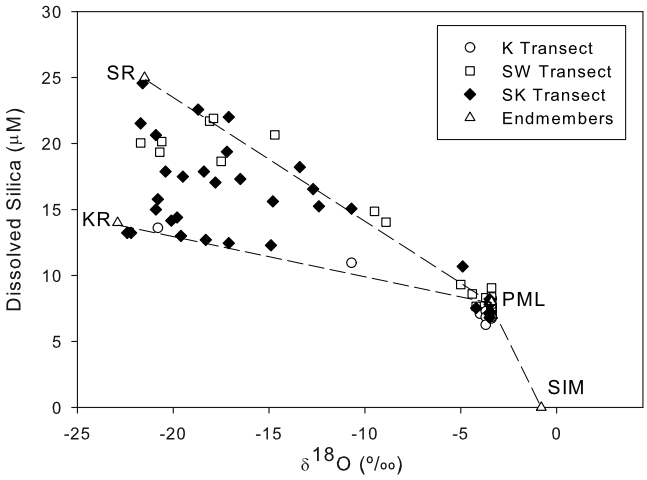

Figure 4. Dissolved silica versus $\delta^{18}O$ for selected stations and depths in Stefansson Sound from 23 to 31 May 2004. End-member values for KR, SR, SIM, and PML are shown by the open triangles and labeled accordingly. Dashed lines connecting the water masses represent simple mixing between end-members.

between the river mixing lines in Figure 4 were from samples with a mixture of SR and KR water (i.e., the SK stations, as described in more detail below). Data points for some of the SW stations plotted below the SR-PML mixing line due to variations in the silica end-member for the SR. As a check on the effect of this variability, numerous runs of the OMP analysis that varied the silica end-member throughout the observed range for the SR were carried out. These calculations altered the calculated water mass fractions by $\leq$10%. Furthermore, data for the K stations, as well as stations SK8, SK9, SK10, and SK6 (closest to KR outflow), plotted on or very close to the KR-PML mixing line, implying little variation in the silica end-member for the KR. We assumed that dissolved silica was essentially conservative in the study area because the seasonal landfast ice cover should restrict growth of phyto-plankton, thereby greatly reducing the amount of biological uptake in the surface water [*Weingartner and Okkonen*, 2001; *Granskog et al.*, 2005]. *Macdonald et al.* [1989] successfully used dissolved silica in combination with salinity and d18 O in a similar water mass analysis for the Mackenzie River estuary in the Canadian Arctic within limited time and space scales.

4.2. SR Plume Water and Sea-Ice Melt

[19] Results from the OMP analysis helped determine the fraction of SR water under ice in Stefansson Sound during the study period. An example of the seaward advancement of the SR plume over time is shown using data from the SW transect for 25 and 28 May (Figures 5a and 5b). On 25 May, the top 1 m of the water column at stations SW1 to SW3 contained 61–84% SR water (Figure 5a). Three days later, an increase in the percent and depth of penetration of SR water was observed along the SW transect (Figure 5b). For

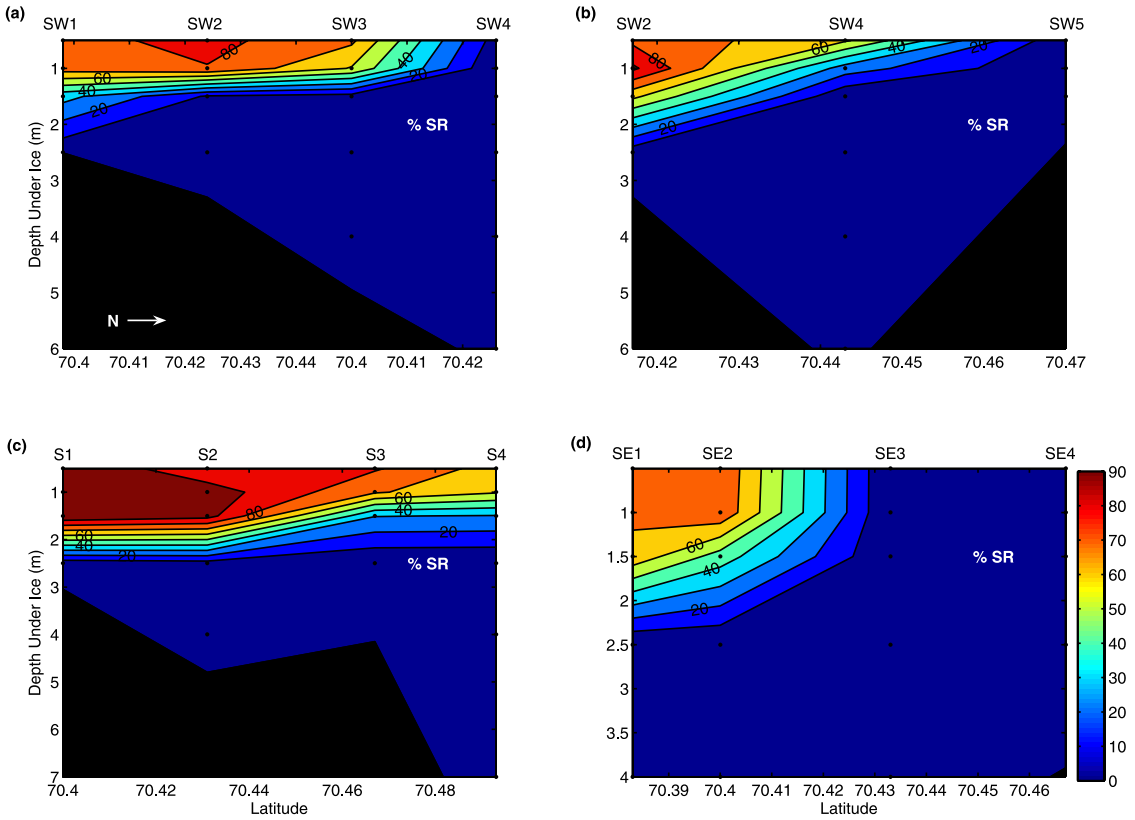

Figure 5. Percent of SR water for (a) SW stations sampled on 25 May, (b) SW stations sampled on 28 May, (c) S stations sampled on 31 May, and (d) SE stations sampled on 27 May. Black shows the seafloor where pertinent. Black dots show sampling depths. Contour interval is 10%.

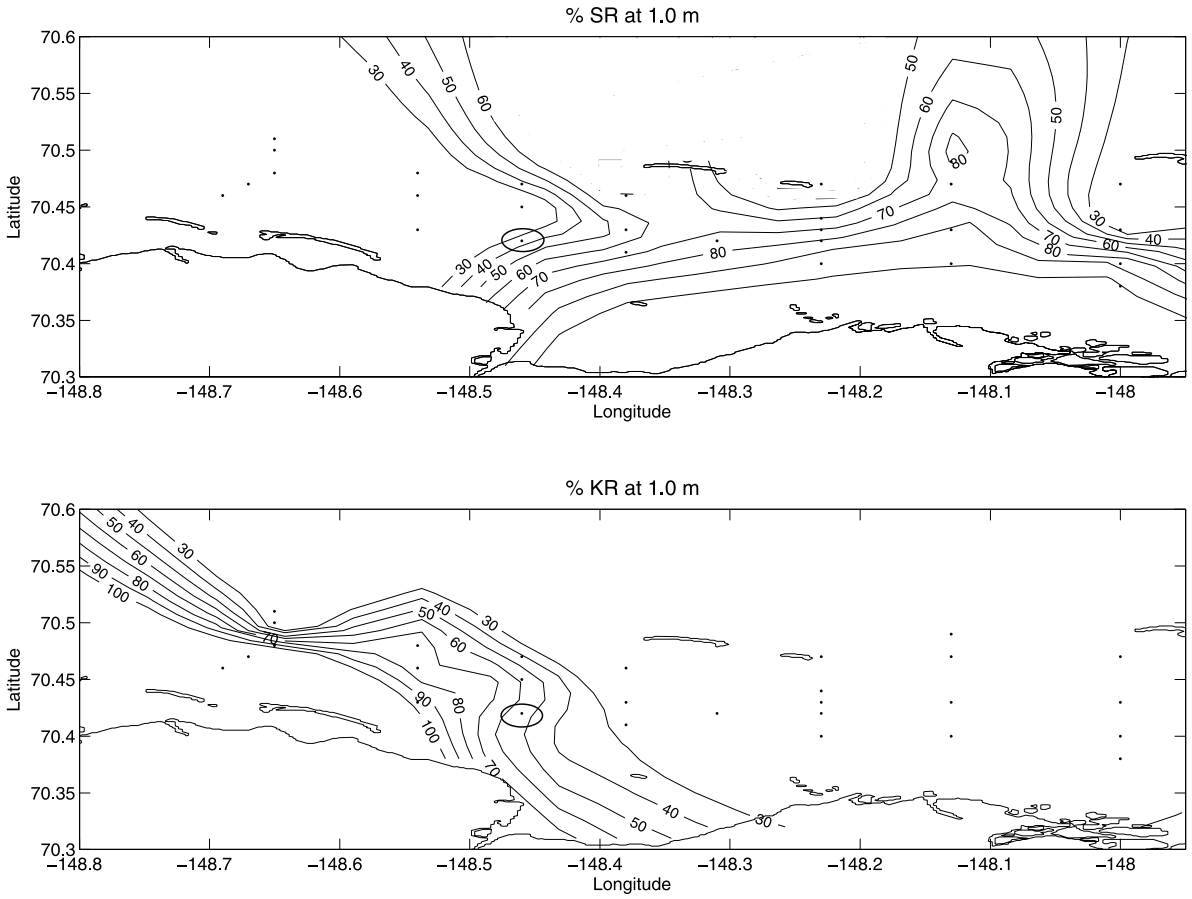

Figure 6. Quasisynoptic view of percent (top) SR water and (bottom) KR water at 1.0 m depth for 27–31 May. Water mass fractions were rounded to the nearest 10%. Station SK5 is circled for orientation.

example, the fraction of SR water increased from 10 to 63% at 1.5 m for station SW2 and from 2 to 29% at 1 m for station SW4 (Figure 5b). The increased fractions of SR water along the SW transect showed both the seaward and vertical progression of the SR plume.

[20] The greatest fractions of SR water ($\geq$90%) were found at depths of 0.5–1.5 m along the S1–S4 transect on 31 May (Figure 5c). The higher fractions of SR water observed along the S transect were partly due to the late (31 May) sample date. However, station SW4, also sampled on 31 May, had a SR water fraction of 62% at 1-m depth. This fraction was similar to values of 73% and 62% (on 31 May) at stations S3 and S4 that were located ~2.7 and 5.6 km farther north, respectively (Figure 1). Therefore the SR plume appeared to progress predominately along the S transect, as discussed in more detail below.

[21] East of the S transect, the SR plume extended ~6.3 km seaward with $\geq$70% SR water in the top 1 m of the water column at stations SE1 and SE2 (Figure 5d). However, no detectable SR water was found at stations SE3 and SE4. Collectively, the OMP results supported movement of the SR plume seaward primarily along the S transect and secondarily along the SW transect with a smaller eastward movement along the SE transect.

[22] A layer of water with a salinity of 25–30 was observed beneath the SR plume at ~2.5 m for all stations. This layer of water, attributed to the entrainment of denser shelf waters into the river-influenced water, limited by the high stratification observed in the water column [*Garvine and Monk*, 1974; *Ingram*, 1981; *Ingram and Larouche*, 1987]. As the plume shoaled and the total water depth increased moving offshore, this water layer widened below the plume and surfaced ahead of the front. The observed trend suggested mixing of SR water with another layer of lower-salinity water that was deeper (>1.5 m) in the water column at stations seaward of the SR plume. This additional source of slightly lower-salinity water was attributed to sea-ice melt that was pulled downward beneath the seaward moving plume front via convergence with a shoreward flow of ambient shelf water [*Garvine and Monk*, 1974; *Ingram*, 1981; *Ingram and Larouche*, 1987; *Macdonald et al.*, 1989]. The percent of SIM was not significant (<10%) in about 70% of the samples because the study was carried out early in the spring melt cycle. Higher fractions of SIM, between 10 and 20%, were calculated at offshore stations K4, K5, SW4, SW5, and SE4 most likely due to greater melting in the vicinity of the offshore barrier islands. Likewise, the calculated contribution of SIM was about 20% at several shallow nearshore stations (SW1, S1, SE1, and SE2).

[23] Overall, results from the OMP analysis suggest that the SR plume was a single, large structure that moved predominately northward along the S and SW transects and spread >15 km to the west and ~5 km to the east of the S

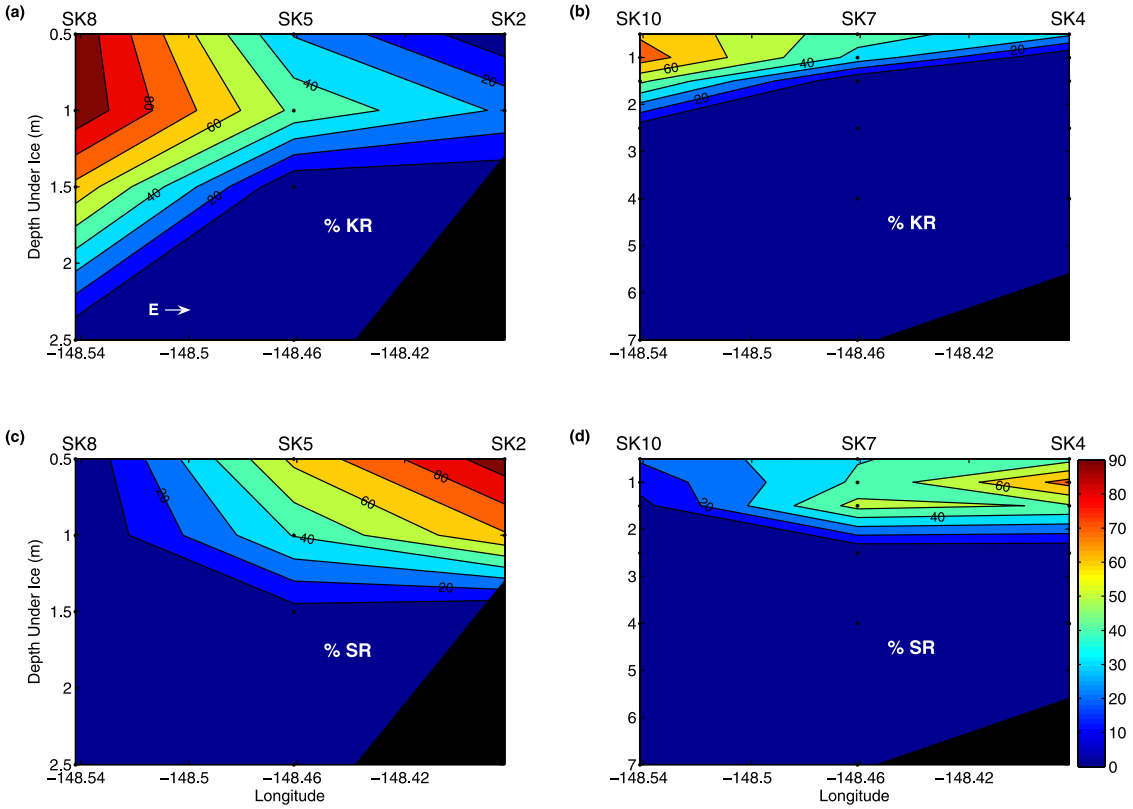

Figure 7. Percent of (a) KR water and (b) SR water for stations SK8, SK5, and SK2, and (c) KR water and (d) SR water for stations SK10, SK7, and SK4. All stations sampled on 30 May. Black shows the seafloor where pertinent. Black dots show sampling depths. Contour interval is 10%.

transect (Figure 6 and discussed in more detail below). The seaward and alongshore spread of the SR plume seemed to be most limited by barrier islands present ~15 km offshore and the KR plume, respectively.

4.3. Sagavanirktok and Kuparuk River Plume Interactions

[24] Results from the SK stations (SK2–SK10), sampled on 29 and 30 May, show the movement of SR water westward as well as the interaction between SR and KR plumes as they converged beneath the ice. Flow from the KR that moved eastward toward the SK stations was channeled by barrier islands and man-made causeways just north of the river mouth that effectively redirected the plume alongshore. Approximately equal fractions of ~40–50% SR and KR water were found in the top 1–1.5 m of the water column at stations SK5 (Figures 7a and 7c) and SK7 (Figures 7b and 7d), where the two plumes met. The distribution of the water mass fractions illustrated in Figure 6 suggest a northward flow of plume water as a result of convergence at or shoreward of station SK5 between the SR plume moving west and the KR plume moving east. For example, the eastward flow of the KR plume from maximum fractions at stations SK8 (Figure 7a) and SK10 (Figure 7b) was driven upward to ~1 m depth by increased mixing with SR water that was moving westward and downward from stations SK2 (Figure 7c) and SK4 (Figure 7d). As a result of the convergence, the KR plume appears to have forced the westward flowing SR water to the north (Figure 6).

[25] No SR water was identified at station SK8 and <20% SR water was found at station SK10 (Figures 7c and 7d). Thus the SR plume did not flow farther west than station SK5, but it was advected north to stations SK6 and SK7 (Figures 6 and 8d). In contrast, KR water was abundant to >2-m depth for stations SK8 to SK10 (Figure 8a) as a result of further redirection northward by the causeway connecting Point McIntyre and the Seawater Treatment Plant to shore (Figure 1) as well as the westward moving SR plume. As a result of mixing between the two plumes along the SK5, SK6, and SK7 transect (meridional), more SR water was advected along the 1.5-m isobath as the SR and KR plumes merged and mixed in the top 1 m of the water column. Furthermore, the decrease in the fraction of KR water east of stations SK8, SK9, and SK10 showed the seaward deflection of the plume because of interaction with the SR water (Figures 8a and 8b). We speculate that the KR plume was mixed more easily by turbulence with the oppositely flowing local circulation. However, the presence of the KR plume was sufficient to force westward spreading SR water north (Figure 6), increasing the possibility of advection to the outer continental shelf. Such interaction among the many rivers along the northern coast of Alaska may aid in the transport of freshwater off the shelf between barrier islands via convergence of alongshore flows.

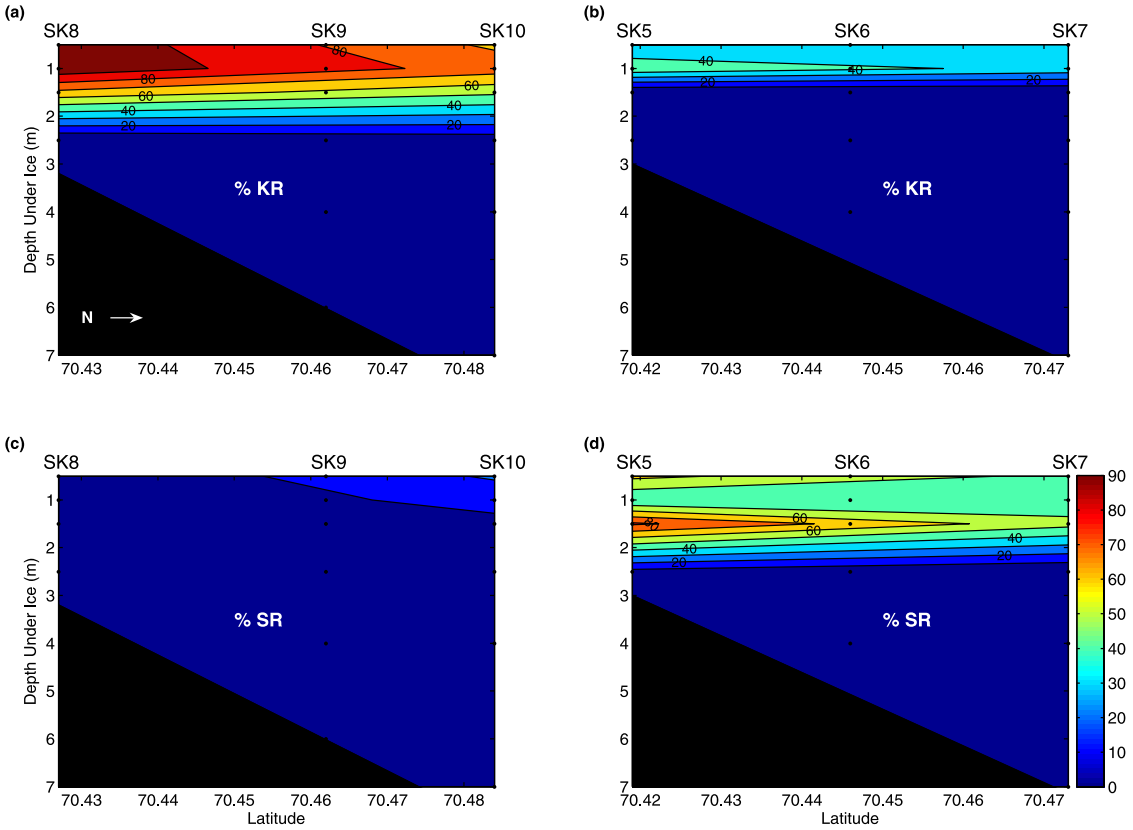

Figure 8. Percent of (a) KR water and (b) SR water for stations SK8, SK9, and SK10, and (c) KR water and (d) SR water for stations SK5, SK6, and SK7. All stations sampled on 30 May. Black shows the seafloor where pertinent. Black dots show sampling depths. Contour interval is 10%.

4.4. Currents

[26] Currents under the ice averaged 7.2 ± 3.2 cm s^{-1} at 309 ± 76° (n = 40). The current data were categorized as surface (1 and 1.5 m) and subsurface (≥2.5 m) on the basis of the observed 1–1.5-m thickness of the SR plume. Surface currents, with an average magnitude of 6 ± 3 cm s^{-1} at 313 ± 115° (n = 17) were not significantly different from subsurface currents that averaged 8 ± 3 cm s^{-1} at 303 ± 34° (n = 23). These results suggest that if a landward flow was present in the top layer of the water column under ice prior to the spring floods, as inferred by *Matthews* [1981] and *Weingartner and Okkonen* [2001], it was reversed during high river discharge. Water flow in Stefansson Sound was northwestward and parallel to the shoreline for the entire study period in agreement with results from *Matthews* [1981] and *Weingartner and Okkonen* [2001]. Exceptions to this trend occurred only where there were mixing fronts, changes in bathymetry, or barrier islands. This was somewhat consistent with the proposed convergence of seaward flowing plume water and shoreward flowing shelf water and possible subduction of shelf water beneath the plume at seaward fronts [*Ingram*, 1981; *Ingram and Larouche*, 1987; *Granskog et al.*, 2005]. Maximum current velocities of ≥10 cm s^{-1} in this study were generally found in regions of plume fronts.

[27] Weak relationships ($r^2 \leq 0.33$) were observed among alongshore and cross-shore current magnitudes, changes in sea level height, and stage height. Thus the observed local circulation was most likely forced by the discharge of river water over the saline shelf water [*Ingram*, 1981; *Ingram and Larouche*, 1987; *Harms et al.*, 2000]. We also observed that the northwestward flow of the local circulation contradicts the usual eastward deflection of northward moving waters because of the Coriolis force. This resultant flow was most likely due to the influence of the high intensity of the river runoff [*Harms et al.*, 2000] as well as possible forcing from the larger-scale anticyclonic Beaufort Gyre offshore [*Weingartner and Okkonen*, 2001].

4.5. Mixing Gradients

[28] Mixing gradients were calculated using the fractions of SR water along isobaths between stations. These gradients helped to quantitatively support qualitative inferences of SR water movement based on the distributions of water mass fractions. Calculations were carried out for the top 1.5 m of the water column where differences in the SR water mass fractions between stations were >10%. Gradients were calculated in % km^{-1} as follows:

$$\text{Gradient}(z) = \left([\%\ \text{River}]_2 - [\%\ \text{River}]_1\right)/L \qquad (1)$$

where flow was assumed to be from station 1 to station 2 (subscripts 1 and 2) along a given sampling depth (z = 0.5, 1, or 1.5 m) and L = distance (in kilometers) between stations. The calculation yielded negative gradients along an assumed flow pathway and positive gradients when

Table 5. Selected Gradients for the Percent of SR Water Between Stations Along 1 m depth

Sample Date	Station 2	SR_2 (%)	Station 1	SR_1, %	$\Delta SR/L$, % km^{-1}
25 May	SK1	31	SR	100	−7
25 May	SK1	31	SW2	80	−15
25 May	SW1	75	SR	100	−3
25 May	SW2	80	SW1	75	-
25 May	SW4	2	SW2	80	−27
25 May	SW3	61	SW2	80	−13
25 May	SW4	2	SW3	61	−41
27 May	S1	70	SR	100	−5
27 May	S1,SE1	70,72	SE1,SE2	72,78	-
27 May	SE1	72	SR	100	−4
27 May	SE3	0	SE2	78	−21
28 May	SK1	76	SR	100	−2
28 May	SK1	76	SW2	92	−5
28 May	SW2	92	SR	100	-
28 May	SW4	29	SW2	92	−22
28 May	SW5	0	SW4	29	−10
30 May	SK2	69	SR	100	−3
30 May	SK5	41	SR	100	−4
30 May	SK5	41	SK2	69	−9
30 May	SK8	0	SK5	41	−13
30 May	SK4	74	SR	100	−2
30 May	SK4	74	SK2	69	-
30 May	SK7	42	SK4	74	−9
30 May	SK7	42	SK5	41	-
30 May	SK10	14	SK7	42	−9
30 May	SK10	14	SK5	41	−3
31 May	S1, S2	99,96	SR, S1	100,99	-
31 May	S3	73	S2	96	−6
31 May	S4	62	S3	73	−4
31 May	SW4	62	S2	96	−9
31 May	SW4	62	SR	100	−3

opposite the proposed flow. The following simplifying assumptions were applied to the gradient calculations: (1) a single source was selected for the SR water at what was believed to be the primary outflow (see Figure 9) and (2) gradient calculations assumed all river water entering the study area did so via only this outflow.

[29] Flow pathways were determined by comparing horizontal gradients (e.g., 1 m, Table 5) and assumed that smaller gradients ($<-5\%$ km^{-1}) represented primary flow pathways and larger gradients ($\geq -10\%$ km^{-1}) represented a resistance to flow or shear that was identified where physical barriers or water mass fronts were present. For example, on 25 May, two possible flow pathways of SR water to station SK1 along the 1 m isobath were chosen, one from the SR mouth ($\Delta SR/L = -69\%/10.5$ km $= -7\%$ km^{-1}) and the other from station SW2 ($\Delta SR/L = -49\%/3.3$ km $= -15\%$ km^{-1}). The two gradients suggested that SR water more likely flowed directly from the mouth of the SR because it would have been less mixed by approximately a factor of two along that route.

[30] The flow pathways determined by comparing horizontal gradients in this manner are shown schematically in Figure 9. Generally, mixing (larger gradients) was comparatively lower in a cross-shore (N-S) versus alongshore (E-W) direction, indicating a preferential seaward advection of SR water. The presence of relatively unmixed SR water ($\geq$90% SR) from the SR mouth to stations closest to the shore (e.g., SK1, SW1, S1, and SE1) indicated a large and increasing pool of SR water located shoreward of these stations. Mixing fronts were consistently observed between stations located farther offshore (e.g., SW4 and SW5) with magnitudes >20% km^{-1}, marking the limits of the spread of SR water. Small mixing gradients ($\leq$4% km^{-1}) observed between the SR mouth and the SK stations confirmed a similarly large westward spread of SR water.

4.6. River Water Budget

[31] A freshwater budget was calculated for the SR discharge using the water mass fractions from the OMP analysis. The total amount of SR water at each station was calculated as an equivalent water depth in meters by assuming the calculated fractions represented actual fractions of SR water in the water column. Fractions of SR water were interpolated between sampling depths. The top 0.5 m of the water column under ice was assumed to be homogeneous. The resulting meters of SR water were integrated over the water column to only 2.5 m because no river water was identified below this depth during the study. Thus, at station SW4 on 31 May, the % SR water was 79% at 0.5 m, 62% at 1.0 m, 47% at 1.5 m, and 0% at 2.5 m to yield an integrated total equivalent of 1.1 m of pure SR water.

[32] The rate of change in estimates of SR water was calculated to be 0.15 ± 0.04 m d^{-1} at stations that were occupied more than once during the study (S1, SW2, SW4, SK1, SK6, and SK8). The rate of SR water accumulation was assumed constant over the study area and used to calculate the total amount of SR water at each station from the most recent occupation to the last day of the study (2 June). Some values were adjusted so that the depth equivalent of SR water was $\leq$2.5 m, and data for stations SK1 and SK2 were adjusted so that values did not exceed their total bottom depths of 1.5 and 1.0 m, respectively (Table 6).

[33] The depth equivalent of SR water at individual stations averaged 1.6 ± 0.7 m. This average value was multiplied by the area of the SR plume ($\sim$315 km^2), to yield a total volume in the study area on 2 June 2004 of 0.5 ± 0.2 km^3. The SR discharge for the study period was calculated as 1 km^3 from daily average streamflow data taken from the *USGS* [2005]. *Rember and Trefry* [2004] noted that this gauge is located $\sim$130 km upstream of the river mouth and receives water from only $\sim$20% of the drainage basin. These assumptions were taken into account in the volume calculations. Consequently, on 2 June, the calculated volume of SR water within the study area accounted for $\sim$50% of the total discharge. The SR discharge observed was low, most likely due to flow outside of the study area and to being unable to sample closer to shore where a large fraction of the river water resided. Furthermore, our calculations represent only water sampled beneath the ice. Typically, a large percentage of Arctic rivers' discharge flows above the ice layer and is controlled primarily by the winds. This water will eventually reenter the water column via strudel holes or during the melt and consequent break up in July [*Walker*, 1998].

5. Conclusions

[34] Salinity, $\delta^{18}O$, and dissolved silica were used to identify, trace, and quantify the movement of Sagavanirktok

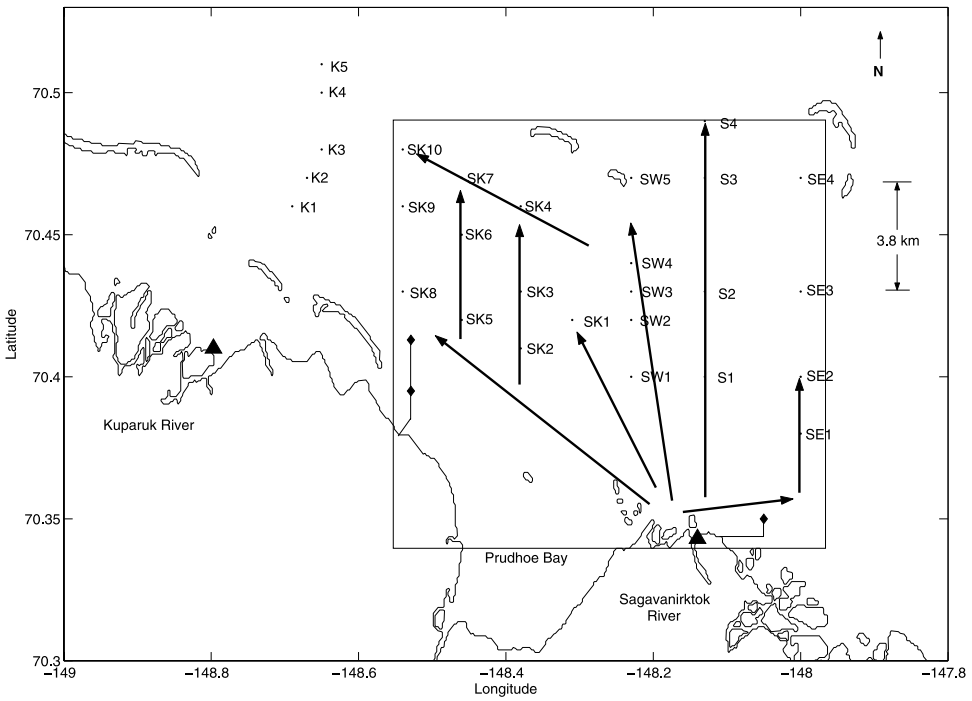

Figure 9. Qualitative flow pathways for SR water according to lowest negative gradients and the calculated area of influence of the SR plume (rectangle). Solid triangles show the locations of the SR and KR outflows in gradient calculations. The lengths of arrows show the extent to which the SR plume was observed.

River (SR) water beneath a 2-m-thick ice layer into the coastal Beaufort Sea. The SR water was transported beneath the ice, relatively undiluted, to a distance of ~6–8-km offshore and ~8–10-km alongshore in ~3 days. Transport of relatively undiluted river water beneath the ice provides a pathway for potential contaminants originating from activities on the North Slope to move offshore.

[35] The SR plume was ~1.0–1.5-m thick with the majority of the river water (≥60%) in the top 1 m over an area of ~315 km^2. The volume of SR water in the study area was calculated as ~0.5 km^3 on 2 June, a value that was ~50% of the total river discharge for the study period. The plume was centered along the S transect and spread from the SR mouth predominately northward (~16.7 km offshore) and westward (~15 km) with the local circulation to the SW and SK stations, but also spread eastward (~5.2 km) to the SE stations.

[36] Interactions between the SR and KR plumes beneath the ice resulted in the KR plume mixing with and flowing above the SR plume in the top 0.5–1 m of the water column. Convergence between the SR and KR plumes created mixing fronts at stations closer to shore (e.g., SK5) that resulted in an increased northward flow of both plume waters. This observation implies that multiple Arctic river plumes may interact to result in stronger northward flows that may have a greater chance of moving off the continental shelf. This may result in a more saline surface layer from which sea ice will form in winter because of a lack of significant winter discharge from the rivers. The distribution of both SIM and spring runoff will thus determine the salinity of the shelf water and winter brines. Although the SR and KR may be too small to significantly affect the freshwater budget of the Arctic Ocean, the details of their discharge, movement off the shelf, and subsequent distribution may significantly improve efforts for the containment and clean up of any industrial spills that may occur on the North Slope as well as enhance understanding of the

Table 6. Contribution of SR Water to Individual Stations on 2 June 2004 Estimated Using an Average Rate of 0.2 m d^{-1}

	Initial, m	Days to 2 June 2004	Final, m	Adjusted Final, m	Percent of SR Total
SW1	1.2	8	2.8	2.5	7
SW2	1.5	5	2.5		7
SW3	0.8	8	2.4		7
SW4	1.1	2	1.5		4
SW5	0.0	5	1.0		3
SE1	1.4	6	2.6	2.5	7
SE2	1.3	6	2.5		7
S1	2.0	2	2.4		7
S2	1.8	2	2.2		6
S3	1.2	2	1.6		5
S4	1.0	2	1.4		4
SK1	1.1	5	2.1	1.5	4
SK2	0.9	3	1.5	1.0	3
SK3	0.8	5	1.8		5
SK4	1.0	3	1.6		5
SK5	1.3	3	1.9		5
SK6	0.4	0	0.4		1
SK7	0.9	3	1.5		4
SK8	0.5	0	0.5		1
SK9	0.4	4	1.2		3
SK10	0.2	3	0.8		2
SUM				34.7	100
AVG				1.6 ± 0.7	

processes that affect brine formation and ventilation of the southern Beaufort Sea halocline.

[37] **Acknowledgments.** We thank Mark Savoie of Kinnetic Laboratories, Inc. for logistical support in the field. We also thank Geochron Laboratories, Inc., and NOAA at the University of Miami for assistance with analyses. We thank Robert D. Rember, Robert P. Trocine, and Debra W. Woodall for their work in the laboratory and in the field. We thank British Petroleum for providing access to and laboratory space on the North Slope. Financial support for this work was derived from the U.S. Department of the Interior, Minerals Management Service, contract 1435-01-04-CT-32080.

References

Aagaard, K., and E. C. Carmack (1989), The role of sea ice and other fresh water in the Arctic circulation, *J. Geophys. Res.*, *94*, 14,485–14,498.

Aagaard, K., L. K. Coachman, and E. C. Carmack (1981), On the halocline of the Arctic Ocean, *Deep Sea Res., Part A*, *28*, 529–545.

Eicken, H., I. Dmitrenko, K. Tyshko, A. Darovskikh, W. Dierking, U. Blahak, J. Groves, and H. Kassens (2005), Zonation of the Laptev Sea landfast ice cover and its importance in a frozen estuary, *Global Planet. Change*, *48*, 55–83.

Garvine, R. W., and J. D. Monk (1974), Frontal structure of a river plume, *J. Geophys. Res.*, *79*, 2251–2259.

Granskog, M. A., J. Ehn, and M. Niemela (2005), Characteristics and potential impacts of under-ice river plumes in the seasonally covered Bothnian Bay (Baltic Sea), *J. Mar. Syst.*, *53*, 187–196.

Grasshoff, K. (1976), *Methods of Seawater Analysis*, 317 pp., Verlag Chemie, New York.

Harms, I. H., M. J. Karcher, and D. Dethleff (2000), Modelling Siberian river runoff—Implications for contaminant transport in the Arctic Ocean, *J. Mar. Syst.*, *27*, 95–115.

Hinrichsen, H. H., and M. Tomczak (1993), Optimum multiparameter analysis of the water mass structure in the western North Atlantic Ocean, *J. Geophys. Res.*, *98*, 10,155–10,169.

Ingram, R. G. (1981), Characteristics of the Great Whale River Plume, *J. Geophys. Res.*, *86*, 2017–2023.

Ingram, R. G., and P. Larouche (1987), Variability of an under-ice river plume in Hudson Bay, *J. Geophys. Res.*, *92*, 9541–9547.

Ingram, R. G., J. Wang, C. Lin, L. Legendre, and L. Fortier (1996), Impact of freshwater on a subarctic coastal ecosystem under seasonal sea ice (southeastern Hudson Bay, Canada). I. Interannual variability and predicted global warming influence on river plume dynamics and sea ice, *J. Mar. Syst.*, *7*, 221–231.

Karstensen, J. (2005), Optimum Multiparameter (OMP) analysis user group, Lamont-Doherty Earth Observatory, Columbia Univ. (Available at http://www.ldeo.columbia.edu/%7Ejkarsten/omp_std/)

Macdonald, R. W., E. C. Carmack, F. A. McLaughlin, K. Iseki, D. M. Macdonald, and M. C. O'Brien (1989), Composition and modification of water masses in the Mackenzie Shelf estuary, *J. Geophys. Res.*, *94*, 18,057–18,070.

Macdonald, R. W., D. W. Paton, and E. C. Carmack (1995), The freshwater budget and under-ice spreading of Mackenzie River water in the Canadian Beaufort Sea based on salinity and $^{18}O/^{16}O$ measurements in water and ice, *J. Geophys. Res.*, *100*, 895–919.

Macdonald, R. W., E. C. Carmack, and D. W. Paton (1999), Using the $\delta^{18}O$ composition in landfast ice as a record of arctic estuarine processes, *Mar. Chem.*, *65*, 3–24.

Mackas, D. L., K. L. Denman, and A. F. Bennett (1987), Least-square multiple tracer analysis of water mass composition, *J. Geophys. Res.*, *92*, 2907–2918.

Matthews, J. B. (1981), Observations of under-ice circulation in a shallow lagoon in the Alaskan Beaufort Sea, *Ocean Manage.*, *6*, 223–234.

Melling, H., and R. M. Moore (1995), Modification of halocline source waters during freezing on the Beaufort Sea shelf: Evidence from oxygen isotopes and dissolved nutrients, *Cont. Shelf Res.*, *15*, 89–113.

National Geophysical Data Center (2005), Coastline extractor, NOAA Sat. and Inf. Serv., Silver Spring, Md. (Available at http://rimmer.ngdc.noaa.gov/mgg/coast/getcoast.html)

Rember, R. D., and J. H. Trefry (2004), Increased concentrations of dissolved trace metals and organic carbon during snowmelt in rivers of the Alaskan Arctic, *Geochim. Cosmochim. Acta*, *68*, 477, doi:10.1016/S0016-7037(03)00458-7.

Sever, M. (2005), Aging Alaska oil pipelines, *Geotimes*, *50*, 44–45.

Thompson, R. O., and R. J. Edwards (1981), Mixing and water mass formation in the Australian Sub-Antarctic, *J. Phys. Oceanogr.*, *11*, 1399–1406.

Tomczak, M. (1981a), An analysis of mixing in the frontal zone of South and North Atlantic Central Water off north-west Africa, *Prog. Oceanogr.*, *10*, 172–192.

Tomczak, M. (1981b), A multiparameter extension of temperature/salinity diagram techniques for the analysis of non-isopycnal mixing, *Prog. Oceanogr.*, *10*, 147–171.

U.S. Geological Survey (USGS) (2005), Water Resources, Real-Time Data for Alaska, gauge #15908000, Anchorage, Alaska. (Available at http://nwis.waterdata.usgs.gov/ak/nwis/discharge/?site_no=15908000&agency_cd=USGS)

Walker, H. J. (1998), Arctic deltas, *J. Coastal Res.*, *14*, 718–738.

Weingartner, T. J., and S. R. Okkonen (2001), Beaufort Sea nearshore under ice currents: Science, analysis and logistics, *Final Rep. OCS Study MMS 2001–068*, Univ. of Alaska Coastal Mar. Inst., University of Alaska Fairbanks, Fairbanks.

M. B. Alkire, College of Oceanic and Atmospheric Sciences, Oregon State University, Corvallis, OR 97330, USA. (malkire@coas.oregonstate.edu)

J. H. Trefry, Department of Marine and Environmental Systems, Florida Institute of Technology, Melbourne, FL 32901–6975, USA.